


Article

3D-Printed Bio-Inspired Mechanisms for Bird-like Morphing Drones

Peter L. Bishay *, Matthew Brody, David Podell, Francisco Corte Garcia, Erik Munoz, Evette Minassian and Kevin Bradley

Department of Mechanical Engineering, California State University, Northridge, CA 91330, USA

* Correspondence: peter.bishay@csun.edu

Featured Application: Unmanned aerial vehicles (UAVs), radio-controlled (RC) drones.

Abstract: Birds have unique flight characteristics unrivaled by even the most advanced drones due in part to their lightweight morphable wings and tail. Advancements in 3D-printing, servomotors, and composite materials are enabling more innovative airplane designs inspired by avian flight that could lead to optimized flight characteristics compared to traditional designs. Morphing technology aims to improve the aerodynamic and power efficiencies of aircraft by eliminating traditional control surfaces and implementing wings with significant shape-changing ability. This work proposes designs of 3D-printed, bio-inspired, non-flapping, morphing wing and tail mechanisms for unmanned aerial vehicles. The proposed wing design features a corrugated flexible 3D-printed structure to facilitate sweep morphing with expansion and contraction of the attached artificial feathers. The proposed tail feather expansion mechanism features a 3D-printed flexible structure with circumferential corrugation. The various available 3D-printing materials and the capability to print geometrically complex components have enabled the realization of the proposed morphing deformations without demanding relatively large actuation forces. Proof-of-concept models were manufactured and tested to demonstrate the effectiveness of the selected materials and actuators in achieving the desired morphing deformations that resemble those of seagulls.



Citation: Bishay, P.L.; Brody, M.; Podell, D.; Corte Garcia, F.; Munoz, E.; Minassian, E.; Bradley, K. 3D-Printed Bio-Inspired Mechanisms for Bird-like Morphing Drones. *Appl. Sci.* **2023**, *13*, 11814. <https://doi.org/10.3390/app132111814>

Academic Editor: Wei Huang

Received: 24 August 2023

Revised: 14 October 2023

Accepted: 23 October 2023

Published: 29 October 2023



Copyright: © 2023 by the authors. Licensee MDPI, Basel, Switzerland. This article is an open access article distributed under the terms and conditions of the Creative Commons Attribution (CC BY) license (<https://creativecommons.org/licenses/by/4.0/>).

Keywords: 3D-printing; unmanned aerial vehicles; morphing aerospace structures

1. Introduction

Commercial aircraft are fixed-winged powered vehicles with discrete control surfaces, such as ailerons, rudders, elevators, and flaps, to control the flight path by altering the generated aerodynamic forces and moments. In contrast, birds have flexible wings that can flap to generate the needed lift and propulsion. Indeed, certain birds can fly for hours without a single flap. This is achieved by the highly efficient aerodynamic performance of birds' wings during gliding and soaring [1]. Birds can dynamically change their wing and tail postures to maximize adaptability and achieve diverse flight behaviors (e.g., maneuvering, gliding, and soaring flight) and flight environments (e.g., dense jungle, urban, and mountain environments) [2]. The deformation of birds' wing posture under aerodynamic loading is a complicated kinematic coupling process, primarily comprising two critical aspects: large-scale geometric wing deformations (e.g., changes in wing area, wingspan, chord length, sweep angle, or wing twist) and small-scale local deformations of each flexible feather (e.g., bending, twisting, and fluttering).

Design concepts of bio-inspired wing configurations can be roughly classified into three major categories: (A) bio-inspired non-deformable wing configurations only considering biological structural elements of birds' wings, such as slotted wing-tips, feather flaps, and non-smooth wing surface features; (B) bio-inspired deformable wing configurations only considering basic morphing motion features, such as variable-camber, variable-sweep,

twisting, folding, and inflatable deformations; (C) complex bio-inspired wing configurations considering biological structural elements and morphing motion modes [1]. Category B is the most common in literature. Multiple review papers have presented the various designs of morphing unmanned aerial vehicles (UAVs) from myriad aspects [3–6]. The superiority of morphing wings over traditional wings has been demonstrated in numerous studies, including the work by Joshi et al. [7]. Recent examples of morphing UAVs include the Transformer Aircraft with span-morphing wings [8], MataMorph-2 with twist-morphing wings [9], and MataMorph-3 with camber-morphing wings and tail stabilizers [10]. Recently, researchers have developed new bio-inspired wing configurations that incorporate the biological structural elements and morphing motion of birds' wings (Category C) [11].

Although UAVs with flapping and non-flapping wing designs have been realized, non-flapping designs are more mature, scalable, arguably more practical, and capable of higher speeds [12]. Flapping designs (ornithopters) have poorer thrust-to-weight ratios and additional dynamic degrees of freedom to allow for flapping, which can lead to more mechanical issues. Examples of non-flapping bio-inspired UAVs include (1) "RoboSwift" (<https://www.roboswift.nl/>, accessed on 22 October 2023), which has a deformable wing structure inspired by discrete feather elements of swift birds that can be dynamically folded into different swept-wing shapes, (2) "LisHawk" [13], inspired by the Northern Goshawk, with sweep-morphing feathered wings and tail, (3) "LisEagle" [14] with wing folding and pitching, and (4) "PigeonBot," inspired by the pigeon [15], with sweep-morphing wings and biological feathers.

While fixed airplane wings have been considerably optimized in the last several decades, the design of each type of morphing wing has challenges. Moreover, no current standards exist for designing such new, innovative, and inspired concepts [16]. The primary challenges facing bio-inspired morphing wing design are system complexity, weight, stability, maintainability, scalability, and controllability. The motion of a bird's wing is highly complex, bending and rotating in six degrees of freedom to facilitate flight. However, achieving this mobility in a drone requires numerous components (servomotors, rods, hinges, etc.). The more components added to make the drone more biologically accurate, the heavier and more complex the drone becomes. Meanwhile, birds are remarkably lightweight with hollow bones and feathers, allowing optimal weight efficiency. Realizing this in a drone has proven difficult due to the near-impossible task of finding such lightweight materials. In addition, lighter materials are generally weaker, making them less likely to hold the drone in the air [17].

Birds have novel aerodynamic traits compared to traditional aircraft beyond morphological control, including complementary wing and tail lift. In traditional aircraft design, the wings and tail can generate lift in opposing directions to produce competing pitch moments around the center of mass. While more dynamically stable than a bio-inspired tail, this induces additional drag, as does the use of a vertical control surface. By comparison, birds cradle their center of mass between the upward lift of their wings and tail [18]. They use their tails to achieve yaw control by pivoting the flat surface, splitting lift into pitch and yaw components. Pitch can be adjusted through planar sweep morphing and varying the angle of attack. Although this design is more efficient, it requires more active control and benefits greatly from morphing. Bio-inspired tail designs have been pursued in small ornithopters, however; hobbyists often use this design out of the need to maximize lift. A four-degree-of-freedom bio-inspired tail on a fixed-wing drone was evaluated in a wind tunnel by Murayama et al. [19] to demonstrate its pitch, roll, and yaw characteristics under various conditions.

Seagulls and albatrosses, two very similar families of bird species, are some of the most adept dynamic soaring and gliding birds in the world. Their non-flapping flight performance highly compensates for their poor flapping. Due to the high aspect ratio of their wings, rapid and efficient level flight is enabled, further aided by their lean, streamlined bodies. Their wing structures have evolved to be light and rigid, two critical

factors influencing flight performance and physical limits. The cross-section profile of a seagull's wing closely resembles an S1223 airfoil [20], optimized for high lift and low drag. Indeed, seagulls have been at the center of tremendous aerodynamic research in recent years, hoping to fully grasp the potential of their biologically-engineered and evolutionary design [21–24]. Another interesting feature in avian flight is using a self-actuated covert flap to mitigate stall conditions over the wing [25]. The covert feathers on birds' wings can lift in response to flow separation during stall conditions, allowing birds to maintain higher angles of attack without losing control. This also results in higher lift efficiency.

With the morphing benefits and challenges considered, this paper presents sweep-morphing feathered wing and tail designs for a bio-inspired drone that benefits from the advances in 3D-printing technology and materials. Lightweight and flexible materials have been combined to construct the various components of the wing and tail designs, including plasticized copolyamide thermoplastic elastomer (PCTPE), thermoplastic polyurethane (TPU), Acrylonitrile Butadiene Styrene (ABS), balsa wood, carbon fiber and glass fiber composites. The wing design features a corrugated flexible PCTPE structure similar to the FishBAC design previously used in the flexible ribs of camber-morphing wings [26]. This design can also be supplemented with a dihedral angle morphing capability for fine-tuning flight characteristics. The proposed tail feather-spread mechanism features a 3D-printed TPU flexible structure with circumferential corrugations. This tail design can also be supplemented with a pitch and tilt mechanism. This article presents the nonlinear computational analyses of the designs and the manufacturing and testing of the proof-of-concept models.

The remainder of the article is organized as follows: Section 2 (Materials and Methods) presents the details of the proposed wing and tail designs. This is followed by Section 3 (Results), which focuses on simulations, manufacturing, and testing. Section 4 (Discussion and Conclusions) includes a final discussion and concludes the paper.

2. Materials and Methods

2.1. Wing Design

Figure 1 shows the details of the proposed wing structure. The primary structure supporting the lift generated and the weight of the wings is an artificial bone structure comprising two 3D-printed ABS-carbonite links that extend from the center of the body. The span or length of this inner wing bone structure is comparable to the inner wing length of a seagull, extending to the elbow at a 15° angle, similar to the common gliding configuration of the seagull [24]. The inner wing is covered by an EPP foam skin with the S1223 airfoil profile, which resembles the seagull's airfoil profile, as was highlighted previously [20]. Its chord and span are 24 cm and 25 cm, respectively, smoothly merging at the fuselage surface.

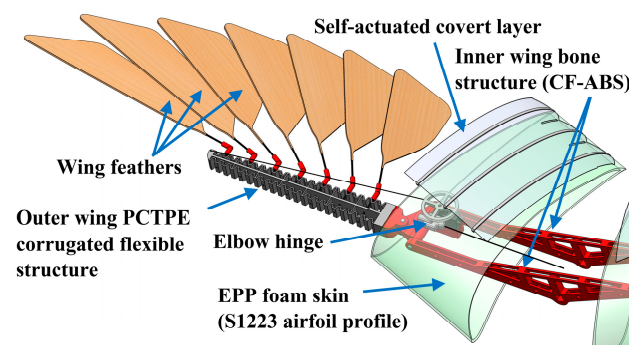


Figure 1. Proposed wing structure.

Sandwiched between the end of the two inner wing bone links, a pivoting elbow hinge is actuated by a servomotor mounted to the fuselage and uses a carbon fiber rod as a pushrod to allow the wing to perform dihedral angle changing motion of the outer wing

(Figure 2). Since this dihedral angle morphing mechanism is uncoupled from the outer wing's feather expansion mechanism, a rigid connection can replace the elbow hinge to increase structural rigidity. Connected to the rotating elbow hinge is a small adapter mated by four short carbon fiber rod connectors, aligning and holding the adapter to the outer wing skeleton (Figure 3).

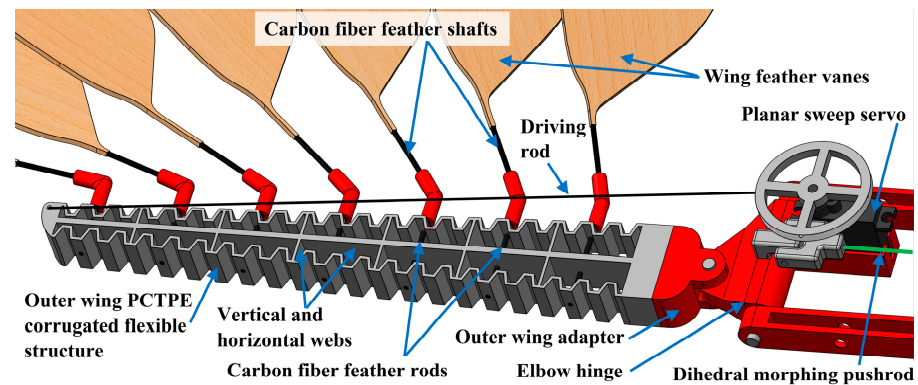


Figure 2. Outer wing skeleton.

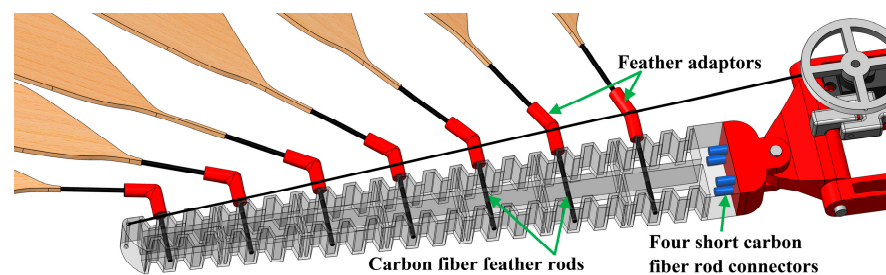


Figure 3. Short carbon fiber rods connect the outer wing adapter to the outer wing corrugated flexible structure.

The outer wing skeleton—the section of the wing where the feathers are attached—is a flexible corrugated structure that resembles the FishBAC design [26] (Figure 2). Vertical and horizontal webs are introduced to add structural support and prevent internal buckling. This corrugated structure allows for tensile expansion of the front and compressive contraction of the back, enabling life-like flexibility in the wing. With carbon fiber feather rods attached through small holes in the front, center, and back walls of the outer wing corrugated flexible skeleton, as shown in Figure 3, the feathers can sweep along the wing's plane when the wing tip is pulled in tension by a servomotor-driven rod. The outer wing skeleton is made of 3D-printed PCTPE. This flexible nylon-based material possesses optimal elastic properties and high ultimate tensile strength. This provides the needed flexibility to flex to the desired shape and spring back to its originally printed position, mimicking the seagull's wing mobility.

The outer wing span with feathers expanded is 50 cm, and with the feathers tucked is 24 cm. The shapes and dimensions of the feathers are based on the Mew Gull feathers, obtained from the U.S. Fish and Wildlife Service's online database (<https://www.fws.gov/lab/featheratlas/>), accessed on 22 October 2023), specifically the P10, P9, and P6–2 feathers of the wing, and the R6–3 and R1 feathers of the tail. P1 is the innermost feather of the primary feather group (on the outer wing); the number increases as the feathers are stacked toward the wing tip. Similarly for the tail, R1 is the tail centermost feather of the rectrices; the number increases moving away from the center. Two options for the artificial feather vane material can be considered: interwoven fiberglass composite ply or reinforced Balsa wood. The composite option is slightly heavier but significantly stiffer and stronger than the Balsa wood option. Feather shafts are 1.5 mm diameter carbon fiber rods.

The self-actuated covert layer (Figures 1 and 4) is simple and lightweight, comprising PCTPE rachides bonded to a ripstop polyester strip attached to the outside of the EPP foam inner wing cover. This design was optimized for weight, simplicity, and ease of integration. If flow begins to separate over the wing, the resultant suction and flow reversal lift the covert surface, stopping the propagation of the flow reversal. Birds have multiple covert feathers for this purpose, resulting in higher performance than a single solid flap [27]. This feather approach allows for a localized response without inducing excess drag from a very large surface lifting into the airstream over the wing. The proposed covert layer design resides between the feather and rigid flap approach and uses a single piece of fabric per wing with local reinforcement from the PCTPE rachides. Minor flap actuation at low angles of attack and excess actuation of rigid flaps have experimentally resulted in efficiency losses during normal flight conditions prior to pressure accumulation near the trailing edge. Experiments have also shown the benefits of low mass and porosity to the flaps' function and sensitivity [27]. The proposed covert design draws inspiration from the longer covert feathers found on seagulls and spans more of the wing chord than its rigid counterparts. It is slightly stiffened by the rachides to prevent unwanted actuation in moderate flight conditions while remaining flexible enough to address flow separation locally. A similar trait exists on the backs of Peregrine falcons, which use covert feathers to prevent flow separation over their backs and tails during rapid descents [28,29]. To prevent pressure accumulation, ridges, and slits are cut into the fabric near the trailing edge, as shown in Figure 4.

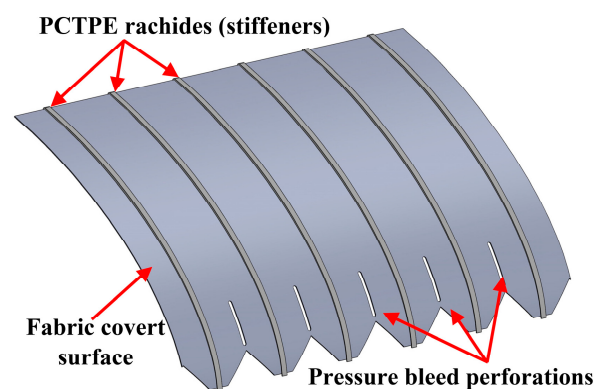


Figure 4. Covert layer structure.

2.2. Tail Design

The proposed tail design is shown in Figure 5a. The compliant feather expansion mechanism is affixed at both ends to an enclosed two-part rigid housing, 3D-printed with ABS, that houses the feather expansion servomotor. This subassembly is mounted on the pitch control servomotor, which sits in a frame directly attached to the tilt servomotor. The tilt servomotor is housed in an ABS bracket connected to the central rod of the drone's fuselage. Similar to the wing design, the pitch and tilt mechanism is uncoupled from the tail's feather expansion mechanism to facilitate its replacement by a rigid connection to increase structural rigidity. The compliant mechanism controls planar feather spread, inspired by the FishBAC mechanism [26] (Figure 5b). 3D-printed TPU offers the best properties for this compliant structure. Linear actuation along a central shaft is converted into radial expansion of the crests to which tail feathers are attached. This design reduces the friction of moving parts in similar designs and maintains kinematic linkage between the tail feathers. The feathers have an innate 5° angle of attack. The structure of the tail feathers is similar to that of the wing feathers.

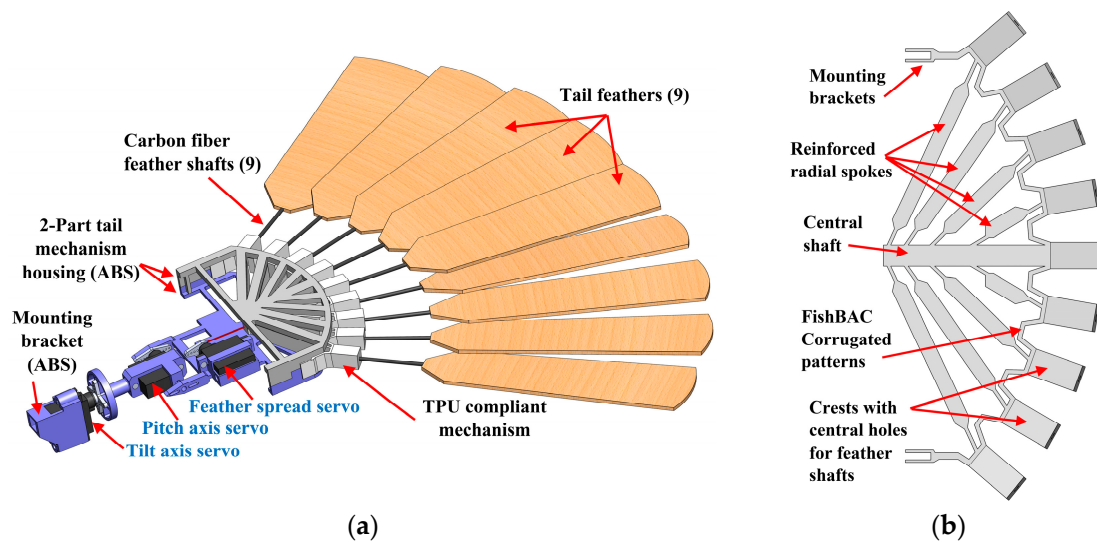


Figure 5. (a) Tail morphing mechanism, (b) TPU compliant mechanism.

The design of the compliant TPU tail feather spread structure was guided by finite element analyses in SOLIDWORKS Simulation, offering the maximum planar feather expansion angle without internal buckling in the radial spokes. The design iterations strategically increased the thickness of a large portion of each spoke (Figure 5b). The results of the converged FEA model showed a maximum planar feather expansion angle change of 46° with a 6 N force applied to the central shaft or a prescribed 10 mm input displacement and a 45° with a 4.4 N force or 6.6 mm prescribed displacement in the opposite direction (detailed in Section 3.1). Compared to the left- and right-hand tail planar morphing design of Murayama et al. [19], symmetric planar morphing was applied. The previously reported paired two DOF morphing control [19] was meant to counteract adverse roll during yaw tilting. This was compensated for by the sweep-morphing wing capabilities.

3. Results

3.1. Finite Element Analyses

The two critical components in the proposed designs were optimized in SOLIDWORKS Simulation for the intended use and to guide the selection of servomotors that would actuate them. The first component is the outer wing PCTPE corrugated structure (Figure 2), and the second is the TPU flexible tail feather expansion structure (Figure 5b). The material properties used in the simulations are listed in Table 1. Due to the large deformations experienced, geometric nonlinearity was considered in solving both models to account for the change in stiffness as the structure is deformed. A convergence study was performed on each component before selecting a suitable mesh; ultimately, a biased mesh refined around smaller features was used.

Table 1. Material properties of the used materials.

	Young's Modulus, E [MPa]	Poisson's Ratio, ν	Yield Strength, σ_y [MPa]
PCTPE	73	0.392	73
TPU	40	0.394	79.3

Due to symmetry, only half the tail structure was modeled, and appropriate symmetry boundary conditions were applied. The structure was fixed at the surface where it contacts the mounting bracket (Figure 5). The converged mesh included 35,194 3D solid elements, corresponding to 58,810 nodes. By applying a 10 mm prescribed displacement to the base of the central shaft, the outer crests extended their spread angle (defined here as the angle between the leftmost and rightmost feathers) from their normal 80° to 126° , a 46°

increase (Figure 6a). Figure 6b shows the factor of safety (FOS) distribution under these conditions. The minimum FOS was 27.24 at one of the corrugations, indicating a safe design during feather expansion actuation. To reduce the feather spread angle by 45°, multiple studies with various downward prescribed displacement values were performed. Only 6.6 mm of downward central shaft displacement was needed to reduce the feather spread angle from 80° to 35° (Figure 6c). In this case, the minimum FOS was 35.16 (Figure 6d), bringing the total tail feather spread actuation range from fully expanded to fully retracted to approximately 91° ($126^\circ - 35^\circ = 91^\circ$).

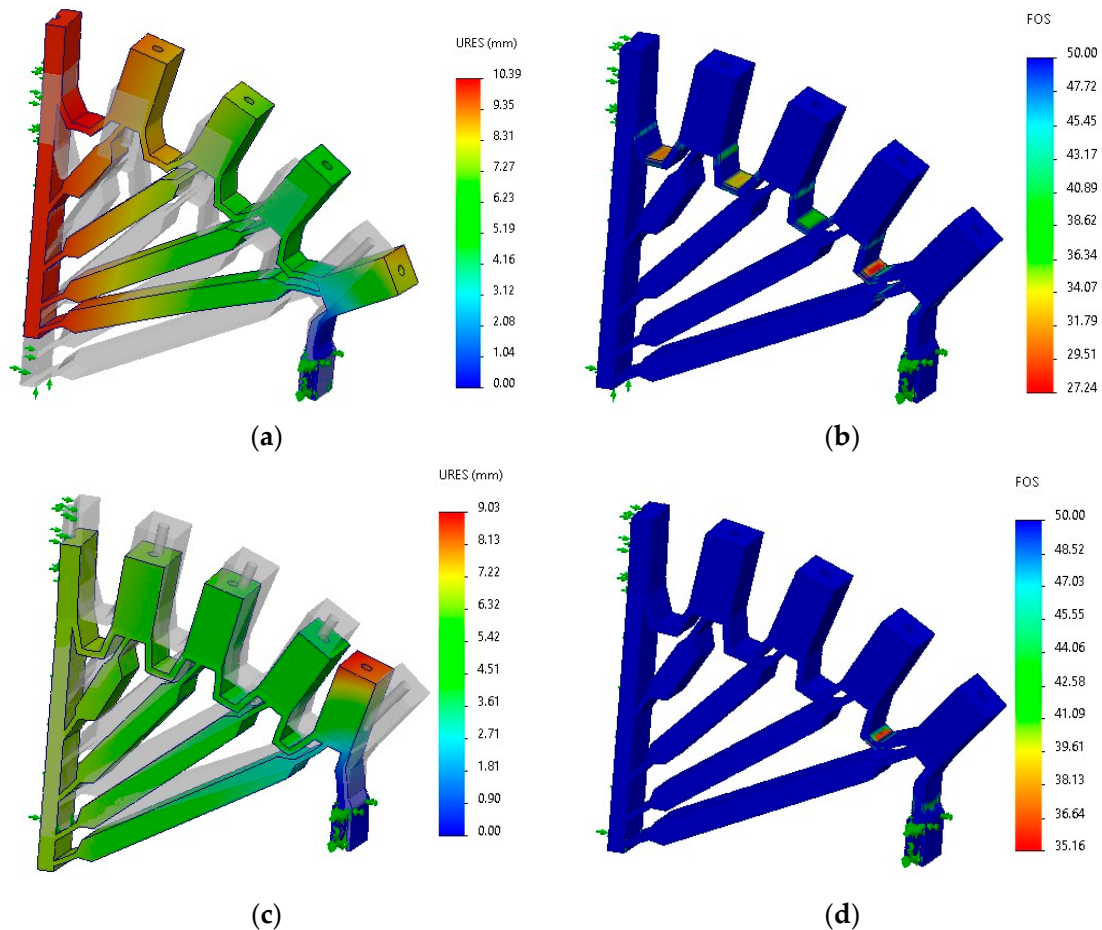


Figure 6. Resultant displacement (URES) and factor of safety (FOS) for the flexible tail feather expansion structure: (a,b) feather expansion, (c,d) feather retraction. The undeformed shapes appear in gray.

The reacting force on the base of the central shaft was 3 N in the feather expansion and 2.2 N in the feather retraction simulations. However, these forces apply to the half model and should be doubled for the full model. Hence, any servomotor providing an output force greater than 6 N is suitable for this mechanism if the stroke is ≥ 10 mm. Higher forces would ensure that any losses or applied loads would not alter the deformed shape of the structure. The selected micro servomotor could provide a torque of up to 4.8 kg.cm. A 1 cm servo horn was used to convert the rotational to linear motion, enabling a 10 mm stroke in both directions. The maximum force would then become $F_{max} = T_{max}/r = 4.8 \times 9.81/1 = 47.1$ N. The minimum torque reported for this servomotor was 4 kg.cm, leading to a minimum force of $F_{min} = T_{min}/r = 4 \times 9.81/1 = 39.2$ N. This relatively large actuation force, which was considerably higher than the required force for morphing (6 N), along with the 10 mm stroke corresponding to the maximum stroke needed for the desired deformed shape, justified the selection of the servomotor, which is also lightweight (8.5 g). Notably, the

aerodynamic transverse loads applied on the feather vanes would be transferred through the feather shafts to this structure. However, the top and bottom solid plates of the tail mechanism housing, which sandwich this feather expansion structure, would provide the needed support. Experimental testing results are provided in Section 3.2.

The outer wing corrugated structure was fixed at the surface contacting the outer wing adapter (Figures 2 and 3). A mesh with 27,321 3D solid elements was used, corresponding to 50,766 nodes. The camber morphing angle was defined as the angle between the tangent line of the tip and the midplane of the corrugated structure. To deform the structure and obtain a 45° camber morphing angle, a 0.4 N vertical force was required at the tip, leading to a maximum resultant displacement of 96.6 mm (Figure 7a). A maximum Von-Mises stress of 3.22 MPa would be generated at the first corrugation closest to the fixture, corresponding to a minimum FOS of 22.7, indicating a safe design at maximum actuation. The angle between the centerline of the structure and the connecting rod where the input force was applied was $\sim 5^\circ$. Hence, the applied force should be $0.4 \text{ N} / \sin(5^\circ) = 4.59 \text{ N}$. Thus, the selected lightweight servomotor, similar to that used for the tail expansion mechanism, would provide sufficient force (at least 39.2 N) to morph the structure via the connecting carbon-fiber rod, maintaining it in its morphed shape for as long as the wing is required to be retracted. For the sake of simplicity, this nonlinear simulation excluded the feathers. Although feathers are relatively lightweight, in flight, the aerodynamic loads applied to the feather vanes are transferred to this corrugated structure via the feather shafts. However, the carbon fiber rod that connects the tip to the servomotor at its root would provide the needed support. Experimental results are presented in Section 3.2.

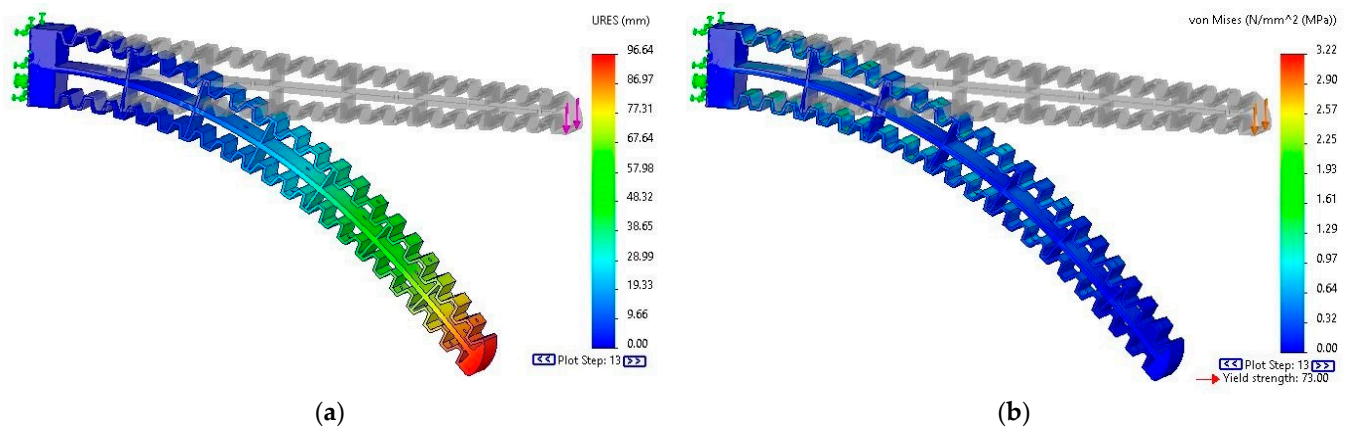


Figure 7. Resultant displacement (a) and Von-Mises stress (b) distributions of the outer wing flexible corrugated structure.

3.2. Manufacturing and Testing

Reinforced balsa wood and interwoven fiber-glass composite laminate were considered for the feathers. Figure 8 shows sample manufactured feathers from both options. Due to its relative simplicity, reinforced balsa wood was selected for the proof-of-concept model. With 3D drawings of all feathers, a laser cutter created the wing and tail feather vanes from 3-mm thick Balsa wood sheets. Carbon-fiber rods of 1.5-mm diameter were used as feather shafts. A strong cyanoacrylate adhesive was applied to bond each shaft to its vane at three points to adjust its orientation. The feathers were then reinforced by a layer of vinyl tape with optimal bidirectional properties for this application. The balsa wood created a solid surface on which aerodynamic forces could act. Meanwhile, the vinyl tape provided reinforcement against bending forces across the wood grains while still keeping the feathers lightweight. The carbon fiber rods offered a lightweight and resilient means of suspending the feathers from their mounting points. The feathers were then inserted into their appropriate pins in the wing or tail subassemblies. Fiber-glass composite feathers, on the other hand, were made of one glass fiber ply taking the outer shape of the feather vane,

and a smaller strip acting as a second ply in central part of the feather. The carbon fiber feather shaft is sandwiched between the two plies, significantly reinforcing the central part of the feather, as shown in Figure 8b.



Figure 8. Sample manufactured feathers: (a) reinforced balsa wood, (b) interwoven fiber-glass composite.

The outer wing's flexible corrugated PCTPE section was 3D-printed, and short 1.5 mm carbon fiber rods were inserted in the holes of its web. Feather adaptors were connected to these rods from one side and the feather shafts from the other. Each adaptor had a different angle to allow the feathers to take the shape of the seagull's outer wing (Figure 9a). The servomotor was placed in its housing in the elbow hinge. The Corona DS-843MG digital high torque micro servo (Torque: 4–4.8 kg.cm, speed 0.12–0.10 s/60°, operating voltage: 4.8–6 V, weight: 8.5 g, dimensions: 23 × 9 × 23 mm) was used for all mechanisms. A carbon fiber rod was connected to the servomotor and ran along the outer wing above the feathers to a connector at the wing tip. The actuation of this servomotor causes wing feather contraction and expansion when the rod is pulled backward and forward, respectively.

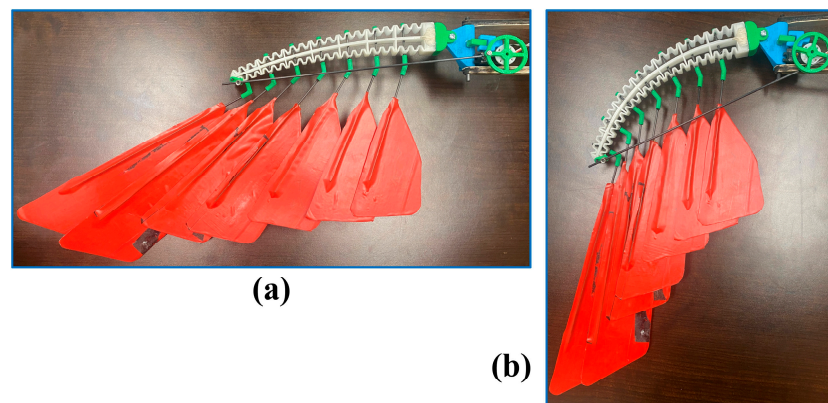


Figure 9. Proof-of-concept model of the proposed outer sweep-morphing feathered wing design: (a) expanded configuration, (b) tucked configuration.

Actuation of the outer wing resulted in a 56.3° camber morphing angle, corresponding to 102 mm of tip vertical deflection (Figure 10a). For comparison, Figure 10b shows the deformed shape from the preliminary finite element analysis, presented in Section 3.1. The camber morphing angle from the simulation was 45°, with 96.6 mm vertical tip deflection. Uncertainty of the material properties used in simulation, manufacturing imperfections, and the slight difference in the applied load's magnitude and direction are possible causes of the difference in the deformed shape between the two models. However, the servomotor, that was selected guided by the simulations, proved to be capable of properly deforming the model to the retracted configuration and support it via the carbon-fiber rod in its morphed configuration. The wing actuation test is presented in Video S1 in the Supplementary Materials.

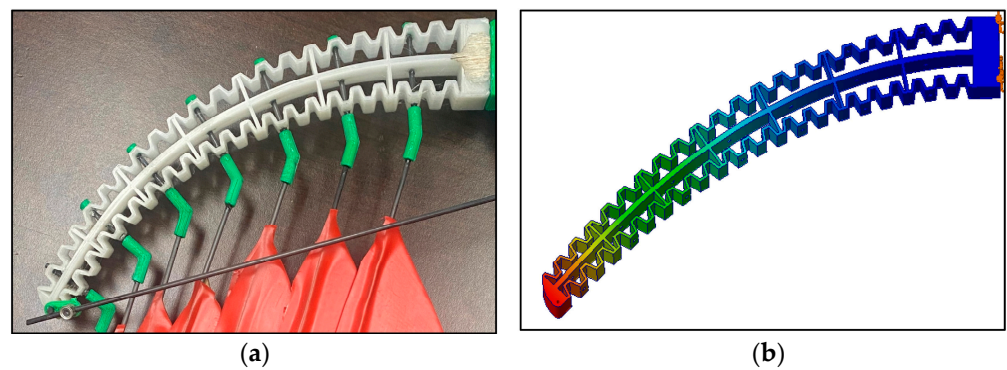


Figure 10. Comparison between the experimental (a) and computational (b) deformations of the outer wing's corrugated structure under actuation force.

The inner wing skin with an S1223 airfoil profile was then wrapped around the inner wing structure to protect it and give the wing its desired aerodynamic profile. The skin was bonded to the fuselage once the final location of the wing was adjusted for stability. The covert layers were bonded to the top surface of the inner wing skin. Figure 9 shows the fully assembled and actuated proof-of-concept model.

The top and bottom parts of the tail mechanism housing were 3D-printed with ABS, stacked, and bonded together. The compliant feather expansion mechanism was 3D-printed with TPU and attached to the housing at both ends. An actuation test was performed by applying an upward displacement of 10 mm and a downward displacement of 6.6 mm to the central shaft, similar to the FEA simulations. A comparison between the experimental and computational results for the expansion, undeformed, and retraction configurations is presented in Figure 11. The tail feather spread angles at these three configurations were 120° , 80° , and 44° , respectively, and the computational spread angles were 126° , 80° , and 35° . Similar to the wing deformation, the difference is possibly due to the uncertainty in material properties and manufacturing imperfections. The computational model proved highly useful in determining the needed stroke from the servomotor and the minimum required actuation force. The computational model was also essential in guiding the design of the spokes to prevent internal buckling.

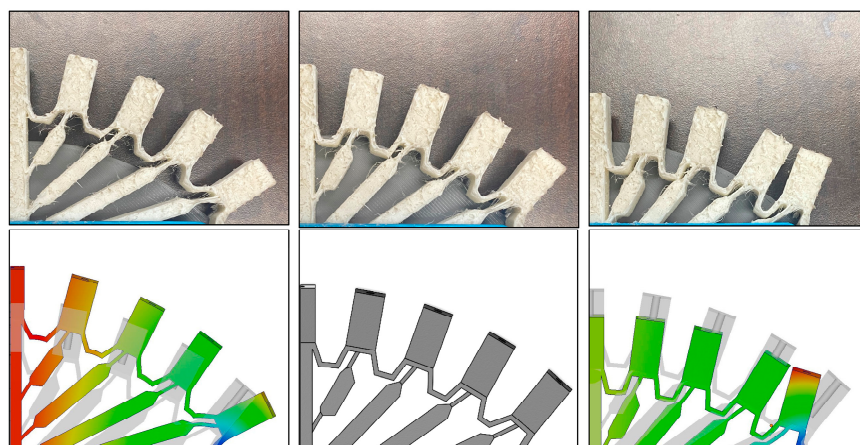


Figure 11. Comparison between the experimental (top) and computational (bottom) deformation of the compliant tail feather expansion structure under actuation in both directions. Left column: expansion (10 mm central shaft upward displacement); middle column: undeformed; right column: retraction (6.6 mm central shaft downward displacement).

The remainder of the tilt and pitch mechanism components were 3D-printed with ABS, and servomotors were installed in their housings to complete the proof-of-concept model (Figure 12). Video S1 in the Supplementary Materials presents the tail actuation test.

The selected servomotors were sufficiently strong to cause the desired actuation, and the selected flexible materials (PCTPE and TPU) proved suitable for these unique applications.

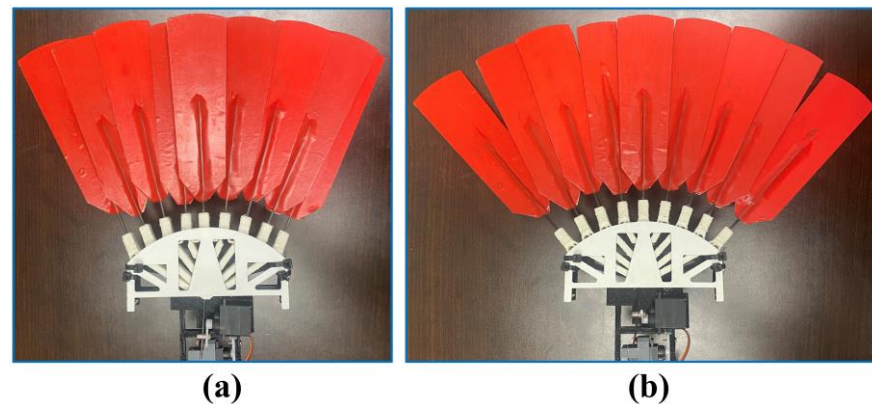


Figure 12. Proof-of-concept model of the proposed sweep-morphing feathered tail mechanism: (a) feather contraction, and (b) feather expansion.

4. Discussion and Conclusions

There are more than 50 species of gulls distributed worldwide, ranging in size from the little gull, at 120 g and 30 cm long, with a 78 cm span, to the great black-backed gull, at 1.75 kg and 76 cm long, with a 1.7 m span. Gulls are generally uniform in shape, with heavy bodies, long wings, and moderately long necks [30]. Bird wings are multifunctional structures with an incredible balance between stiffness to withstand the varying aerodynamic load and flexibility to allow for morphing required for maneuvering. The wings have joints and muscles that enable them to change the orientation of their bones and expand their feathers. Bird bones are lightweight due to their porosity and low density, while feathers are super lightweight yet very strong and durable due to their associated fibers. Indeed, the benefits and superiority of morphing avian wings have been reported compared to traditional ones. However, despite advances in additive manufacturing, composite materials, and servomotors, constructing lightweight, functional morphing UAVs remains technically challenging.

This paper expands on the developments of morphing technology with proposed sweep-morphing feathered wing and tail designs influenced by the anatomy of a common seagull. As highlighted by Baliga et al. [31] and Harvey et al. [20,21], the manipulation of two skeletal joints in the gull's wing (elbow and wrist) is responsible for most of the wing shape change. Hence, the proposed morphing wing design features planar sweep-morphing capability with feather expansion. This morphing action can operate symmetrically or asymmetrically. Asymmetric sweep-morphing generates roll moment. The musculoskeletal mechanism birds use to expand the feathers of their tails was described by Gatesy and Dial [32] and Zusi and Gill [33]. Both highlighted the importance of the bulbi retractor muscle, which holds the root ends of the feathers and acts independently of other tail muscles [33]. As the bulbi retractor contracts, it changes shape, causing the rotational position of each feather to change. The tail feather expansion-compliant mechanism presented in this work mimicked this action to control the rotational position of the tail feather shafts.

Achieving the optimal balance between flexibility, to allow morphing with the available actuation forces, and stiffness/strength, to carry the applied aerodynamic loads, is one of the most challenging tasks in designing morphing structures. Using rigid materials in morphing designs requires a relatively large number of components connected with joints, which could increase friction, complexity, and failure mechanisms. The 3D-printed materials proposed in this work and the geometric design of the wing and tail feather expansion mechanisms proved effective in producing the desired morphing deformations with the available servomotor actuation forces. In both designs, only one component was

needed to hold all feathers and morph them once actuated, avoiding any mechanical joints in the design.

The computational simulations and actuation tests performed on the manufactured proof-of-concept models justified the design decisions and demonstrated the effectiveness of the proposed designs. However, feathers are attached to these mechanisms, and the feather shafts act as cantilever beams that will bend under the transverse aerodynamic load the UAV would experience, depending on the shaft and the vane materials. The proposed shafts are composite rods with two options for the vane material. The laminated composite vanes would be stiffer with a small weight penalty. Further wind tunnel and flight tests on a full UAV would confirm these preliminary findings.

Future work will focus on designing, building, and testing a bio-inspired, non-flapping gull-like drone that implements the proposed wing and tail designs with no traditional flight control surfaces or a vertical stabilizer. The drone's flight dynamics, controllability, and stability will be studied by considering the morphing actuation.

Supplementary Materials: The following supporting information can be downloaded at: <https://www.mdpi.com/article/10.3390/app132111814/s1>, Video S1: Wing and tail actuation.

Author Contributions: Conceptualization, P.L.B., M.B., D.P. and F.C.G.; methodology, all authors; software, all authors; validation, P.L.B., M.B., D.P. and F.C.G.; formal analysis, P.L.B., M.B., D.P., F.C.G. and K.B.; investigation, all authors; resources, P.L.B.; data curation, P.L.B., M.B., D.P., F.C.G. and E.M. (Erik Munoz); writing—original draft preparation, all authors; writing—review and editing, P.L.B., M.B. and D.P.; visualization, P.L.B., M.B., D.P., E.M. (Erik Munoz) and E.M. (Evette Minassian); supervision, P.L.B.; project administration, P.L.B., M.B., D.P. and F.C.G.; funding acquisition, P.L.B. All authors have read and agreed to the published version of the manuscript.

Funding: This research received no external funding.

Institutional Review Board Statement: Not applicable.

Informed Consent Statement: Not applicable.

Data Availability Statement: Data presented in this study are available on request from the corresponding author.

Acknowledgments: This work was performed by the seventh cohort of “Smart Morphing Wing” research-based senior design project at California State University, Northridge (CSUN). The authors acknowledge the support of the following members: Scott Massey, Pratna Chhuon, Dylan Lyon, Narek Gharibi, Paola Ramos, Maaz Umer, Brian Sanchez, and Thurston Gallardo. The authors also thank Felix Schaller for providing academic resources related to self-actuating aerodynamic systems. The authors acknowledge the Mechanical Engineering Department, the Instructionally Related Activities (IRA) grant, and the Student Travel and Academic Research (STAR) program at CSUN.

Conflicts of Interest: The authors declare no conflict of interest.

References

1. Han, J.; Hui, Z.; Tian, F.; Chen, G. Review on Bio-Inspired Flight Systems and Bionic Aerodynamics. *Chin. J. Aeronaut.* **2021**, *34*, 170–186. [[CrossRef](#)]
2. Barbarino, S.; Bilgen, O.; Ajaj, R.M.; Friswell, M.I.; Inman, D.J. A Review of Morphing Aircraft. *J. Intell. Mater. Syst. Struct.* **2011**, *22*, 823–877. [[CrossRef](#)]
3. Sofla, A.Y.N.; Meguid, S.A.; Tan, K.T.; Yeo, W.K. Shape Morphing of Aircraft Wing: Status and Challenges. *Mater. Des.* **2010**, *31*, 1284–1292. [[CrossRef](#)]
4. Min, Z.; Kien, V.K.; Richard, L.J.Y. Aircraft Morphing Wing Concepts with Radical Geometry Change. *IES J. Part A Civ. Struct. Eng.* **2010**, *3*, 188–195. [[CrossRef](#)]
5. Gomez, J.C.; Garcia, E. Morphing Unmanned Aerial Vehicles. *Smart Mater. Struct.* **2011**, *20*, 103001. [[CrossRef](#)]
6. Sun, J.; Guan, Q.; Liu, Y.; Leng, J. Morphing Aircraft Based on Smart Materials and Structures: A State-of-the-Art Review. *J. Intell. Mater. Syst. Struct.* **2016**, *27*, 2289–2312. [[CrossRef](#)]
7. Joshi, S.; Tidwell, Z.; Crossley, W.; Ramakrishnan, S. Comparison of Morphing Wing Strategies Based upon Aircraft Performance Impacts. In Proceedings of the 45th AIAA/ASME/ASCE/AHS/ASC Structures, Structural Dynamics & Materials Conference, Palm Springs, CA, USA, 19–22 April 2004.

8. Ajaj, R.M.; Jankee, G.K. The Transformer Aircraft: A Multimission Unmanned Aerial Vehicle Capable of Symmetric and Asymmetric Span Morphing. *Aerosp. Sci. Technol.* **2018**, *76*, 512–522. [[CrossRef](#)]
9. Schlup, A.; Bishay, P.; Mclennan, T.; Barajas, C.; Talebian, B.; Thatcher, G.; Flores, R.; Perez-Norwood, J.; Torres, C.; Kibret, K.; et al. MataMorph 2: A New Experimental UAV with Twist-Morphing Wings and Camber-Morphing Tail Stabilizers. In Proceedings of the AIAA Scitech 2021 Forum, Virtual, 11 January 2021.
10. Bishay, P.L.; Kok, J.S.; Ferrusquilla, L.J.; Espinoza, B.M.; Heness, A.; Buendia, A.; Zadoorian, S.; Lacson, P.; Ortiz, J.D.; Basilio, R.; et al. Design and Analysis of MataMorph-3: A Fully Morphing UAV with Camber-Morphing Wings and Tail Stabilizers. *Aerospace* **2022**, *9*, 382. [[CrossRef](#)]
11. Harvey, C.; Gamble, L.L.; Bolander, C.R.; Hunsaker, D.F.; Joo, J.J.; Inman, D.J. A Review of Avian-Inspired Morphing for UAV Flight Control. *Prog. Aerosp. Sci.* **2022**, *132*, 100825. [[CrossRef](#)]
12. Mackenzie, D. A Flapping of Wings. *Science* **2012**, *335*, 1430–1433. [[CrossRef](#)]
13. Ajanic, E.; Feroskhan, M.; Mintchev, S.; Noca, F.; Floreano, D. Bioinspired Wing and Tail Morphing Extends Drone Flight Capabilities. *Sci. Robot.* **2020**, *5*, eabc2897. [[CrossRef](#)] [[PubMed](#)]
14. Ajanic, E.; Feroskhan, M.; Wüest, V.; Floreano, D. Sharp Turning Maneuvers with Avian-Inspired Wing and Tail Morphing. *Commun. Eng.* **2022**, *1*, 34. [[CrossRef](#)]
15. Chang, E.; Matloff, L.Y.; Stowers, A.K.; Lentink, D. Soft Biohybrid Morphing Wings with Feathers Underactuated by Wrist and Finger Motion. *Sci. Robot.* **2020**, *5*, eaay1246. [[CrossRef](#)]
16. Ajaj, R.M.; Beaverstock, C.S.; Friswell, M.I. Morphing Aircraft: The Need for a New Design Philosophy. *Aerosp. Sci. Technol.* **2016**, *49*, 154–166. [[CrossRef](#)]
17. Parker, G.; Borbone, J. Wing and Gliding Dynamics of a Flapping Winged Ornithopter. In Proceedings of the 2010 World Automation Congress, Kobe, Japan, 19–23 September 2010; pp. 1–5.
18. Usherwood, J.R.; Cheney, J.A.; Song, J.; Windsor, S.P.; Stevenson, J.P.J.; Dierksheide, U.; Nila, A.; Bomphrey, R.J. High Aerodynamic Lift from the Tail Reduces Drag in Gliding Raptors. *J. Exp. Biol.* **2020**, *223*, jeb214809. [[CrossRef](#)]
19. Murayama, Y.; Nakata, T.; Liu, H. Aerodynamic Performance of a Bird-Inspired Morphing Tail. *J. Biomech. Sci. Eng.* **2023**, *18*, 22-00340. [[CrossRef](#)]
20. Liu, T.; Kuykendoll, K.; Rhew, R.; Jones, S. Avian Wings. In Proceedings of the 24th AIAA Aerodynamic Measurement Technology and Ground Testing Conference, Portland, OR, USA, 28 June 2004.
21. Shepard, E.L.C.; Williamson, C.; Windsor, S.P. Fine-Scale Flight Strategies of Gulls in Urban Airflows Indicate Risk and Reward in City Living. *Phil. Trans. R. Soc. B* **2016**, *371*, 20150394. [[CrossRef](#)]
22. Harvey, C.; Baliga, V.B.; Lavoie, P.; Altshuler, D.L. Wing Morphing Allows Gulls to Modulate Static Pitch Stability during Gliding. *J. R. Soc. Interface* **2019**, *16*, 20180641. [[CrossRef](#)]
23. Harvey, C.; Baliga, V.B.; Goates, C.D.; Hunsaker, D.F.; Inman, D.J. Gull-Inspired Joint-Driven Wing Morphing Allows Adaptive Longitudinal Flight Control. *J. R. Soc. Interface* **2021**, *18*, 20210132. [[CrossRef](#)]
24. Harvey, C.; Inman, D.J. Gull Dynamic Pitch Stability Is Controlled by Wing Morphing. *Proc. Natl. Acad. Sci. USA* **2022**, *119*, e2204847119. [[CrossRef](#)]
25. Meyer, R.; Hage, W.; Bechert, D.W.; Schatz, M.; Knacke, T.; Thiele, F. Separation Control by Self-Activated Movable Flaps. *AIAA J.* **2007**, *45*, 191–199. [[CrossRef](#)]
26. Bishay, P.L.; Finden, R.; Recinos, S.; Alas, C.; Lopez, E.; Aslanpour, D.; Flores, D.; Gonzalez, E. Development of an SMA-Based Camber Morphing UAV Tail Core Design. *Smart Mater. Struct.* **2019**, *28*, 075024. [[CrossRef](#)]
27. Bechert, D.W.; Bruse, M.; Hage, W.; Meyer, R. Fluid Mechanics of Biological Surfaces and Their Technological Application. *Naturwissenschaften* **2000**, *87*, 157–171. [[CrossRef](#)]
28. Ponitz, B.; Triep, M.; Brücker, C. Aerodynamics of the Cupped Wings during Peregrine Falcon’s Diving Flight. *Open J. Fluid Dyn.* **2014**, *4*, 363–372. [[CrossRef](#)]
29. Ponitz, B.; Schmitz, A.; Fischer, D.; Bleckmann, H.; Brücker, C. Diving-Flight Aerodynamics of a Peregrine Falcon (Falco Peregrinus). *PLoS ONE* **2014**, *9*, e86506. [[CrossRef](#)] [[PubMed](#)]
30. Pons, J.-M.; Hassanin, A.; Crochet, P.-A. Phylogenetic Relationships within the *Laridae* (Charadriiformes: Aves) Inferred from Mitochondrial Markers. *Mol. Phylog. Evol.* **2005**, *37*, 686–699. [[CrossRef](#)] [[PubMed](#)]
31. Baliga, V.B.; Szabo, I.; Altshuler, D.L. Range of Motion in the Avian Wing Is Strongly Associated with Flight Behavior and Body Mass. *Sci. Adv.* **2019**, *5*, eaaw6670. [[CrossRef](#)]
32. Gatesy, S.M.; Dial, K.P. From Frond to Fan: *Archaeopteryx* and the Evolution of Short-Tailed Birds. *Evolution* **1996**, *50*, 2037–2048. [[CrossRef](#)]
33. Zusi, R.L.; Gill, F.B. The Marvelous Tail of *Loddigesia mirabilis* (Trochilidae). *Auk* **2009**, *126*, 590–603. [[CrossRef](#)]

Disclaimer/Publisher’s Note: The statements, opinions and data contained in all publications are solely those of the individual author(s) and contributor(s) and not of MDPI and/or the editor(s). MDPI and/or the editor(s) disclaim responsibility for any injury to people or property resulting from any ideas, methods, instructions or products referred to in the content.